RSC Advances

ROYAL SOCIETY OF CHEMISTRY

www.rsc.org/advances

Use for Table of Content only

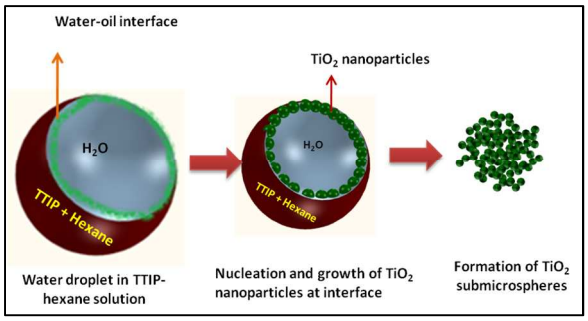

Mechanism for formation of TiO_2 submicrosphere via spray-hydrolysis of micrometric aqueous droplet; hydrolysis reaction occurs at water-hexane interface.

A facile Fabrication of uniform and homogeneous CNT-TiO_2 Composite: A Microscopic and Scattering Investigation

J. Bahadur[1*], J. Prakash[2], D. Sen[1], S. Mazumder[1], P. U. Sastry[1], B. Paul[3], J.K.Chakravartty[2], H. Lammel[4]

([1]Solid State Physics Division, [2]Powder Materials Processing Division, [3]Materials Processing Division) Bhabha Atomic Research Centre, Mumbai, 400085, India

[4]Institut Laue-Langevin, Grenoble Cedex 9, France

Abstract

We demonstrated a facile and robust two-step method to fabricate carbon nanotube/titania nano composite using spray hydrolysis and chemical vapour deposition (CVD) technique with control over morphology and deposition chemistry of reaction. Hierarchically structured NiO doped TiO_2 submicrospheres have been realized by hydrolysis of titanium alkoxide at water-oil interface of micrometer sized droplet. Utilizing these TiO_2 microspheres, composite of TiO_2/CNT has been synthesized through CVD technique. Mesoscopic structural investigations have been carried out on composites using ultra small-angle neutron scattering, small-angle x-ray scattering. There exists three distinct length scales in the composite microspheres. Thermal evolution of microstructure was investigated by in-situ X-ray diffraction which clearly indicates an amorphous to crystalline transition of TiO_2. It is established that the polymorphic phase transition of TiO_2 nanoparticles is associated with the increase in its size. Microscopic studies showed that the TiO_2 substrate has given uniform growth surface for CNT. Further their growth mechanism has been discussed.

*Corresponding Author: jbahadur@barc.gov.in

Keywords: *Spray hydrolysis, TiO_2-CNTs, SAXS, USANS*

1. Introduction

In recent years, titania (TiO_2) has been in the forefront of materials research due to its crucial applications [1-3] in solar cells, portable lithium ion batteries, hydrogen storage etc. Further, it has drawn a lot of interest in photocatalytic degradation of toxic and non-biodegradable organic effluents for decontamination of waste water and environment purification [4-11]. Titania exists in three crystalline forms anatase, rutile and brookite [12]. Anatase and brookite are metastable phases, which irreversibly transform to a stable rutile phase [12]. Recently, it has been shown [13] that anatase to rutile transformation could be arrested by fabricating TiO_2/SiO_2 nanocomposite via evaporation induced self-assembly [14].

Carbon nanotube-titania (CNT/ TiO_2) composites are currently being considered for several applications including their potential use to address environmental problems. Taking advantage of the large surface area, high electrical conductivity and mechanical strength as well as thermal stability of CNTs, the CNT/TiO_2 composites are being utilized in a wide range of applications concerning energy and environment [15], such as, batteries [16], super-capacitors [17, 18], opto-electronics [19], electro-catalysis [20, 21], photo-catalysis [22, 23], sensing devices [24] etc. The primary mechanisms for enhanced photo-catalysis in CNT/TiO_2 composites are discussed in detail by Woan et al. [25].

There are various methods available for the fabrication of CNT/TiO_2 nanocomposites, including the method of attaching nanoparticles (NPs) on wall of CNTs involving covalent or non-covalent interactions [15, 26]. The other most common method is sol-gel route [27, 28]. Hydrothermal method [29] is also utilized for synthesis of CNT/TiO_2 composite. In the sol-gel technique, CNTs are dispersed in a liquid medium. The biggest challenge in this regard is to disperse the CNTs in medium such as, alcohol [30] containing TiO_2 precursor. Most common precursors for

this purpose are metal alkoxides, $(R\text{-}O\text{-})_4Ti$. The dispersion of CNTs and alkoxide in liquid medium plays an important role in deciding the nature and function of the nanocomposite. Further, in sol-gel technique, homogenous nucleation and growth of TiO_2 NPs on CNTs are important and challenging issues.

Owing to the challenges involve in synthesis of uniform and homogeneously dispersed CNT in titania matrix composite, In the present work, we have reported a two-step facile method for fabrication of CNT/TiO_2 without dispersing CNTs in liquid medium, thus avoiding the issues related to heterogeneous nucleation of TiO_2 on CNTs. In present method, first NiO doped TiO_2 is synthesized using the spray hydrolysis technique. This technique is a more controlled method for obtaining the microspheres of the TiO_2 NPs as compared to conventional sol-gel technique. The resulting Ni-TiO_2 composite is used for the substrate material for growing CNTs using a chemical vapor deposition (CVD) technique. Nickel (Ni) acts as a catalyst for growth of CNTs.

First, Nagamine et al. reported a simple method for preparing TiO_2 microsphere. In this method water is sprayed, onto titanium tetraisopropoxide (TTIP) [31] .This method of spray hydrolysis has several advantages as compared to other existing methods due to availability of large surface area for hydrolysis reaction at the interface of the droplet. It is worthy to mention here that concentration of TTIP at droplet interface plays a crucial role and in turn decides the morphology of the resulting TiO_2 grains [31, 32]. It is expected that rapid hydrolysis of TTIP at interface between water droplet and organic phase may lead to the formation of TiO_2 shell if concentration of TTIP is small leading to formation of micrometer sized hollow grains [31]. However, it has been shown [32] that shell formation does not occur for larger concentration of TTIP and leads to formation of sub-micrometric grains. Hydrophilic substances may easily be encapsulated just by spraying their aqueous solutions. This feature of the spray hydrolysis

method has been utilized to prepare doped TiO_2 microspheres having varying functionality [33, 34].

Present work deals with a novel synthesis method of CNT/TiO_2 nanocomposites using spray hydrolysis and CVD technique. Further, mesoscopic structures of hydrolyzed TiO_2 grains and its CNT composites have been studied by small angle X-ray scattering (SAXS) and ultra small angle neutron scattering (USANS) techniques in conjunction with electron microscopy. Thermal evolution of the crystalline phases of titania has been probed using X-ray diffraction. The microscopic structure of composite were studied using SEM and TEM. A plausible mechanism for the formation of TiO_2 submicrosphere has also been elucidated.

2. Experimental Section

2.1. Spray Hydrolysis

Nickel nitrate solutions, with different stoichiometric amount of nickel, have been prepared in 5 ml de-ionized water. The nitrate solution was atomized and sprayed using a two fluid nozzle. Spray droplets were feed into a mixture, containing 10 ml of titanium iso-propoxide (TTIP) and 90 ml of Hexane, kept under stirring (Fig. 1).The typical distance from the nozzle to solution was 15 cm. Stirring rate during reaction was 500 rpm. The reaction was performed at room temperature. Size of the droplet, generated by two fluid jet nebulizer, depends on the atomization pressure [35]. In present work, the atomization pressure was kept 1 Kg/cm^{-2}. The typical droplet size for this pressure is 20 micron.

A greenish color precipitates obtained within a few seconds. Resulting precipitates was filtered, washed and dried. The precipitates were dried overnight under ambient condition. Concentrations of $Ni(NO_3)_2$ have been chosen in such a way that Ni weight remains as 2, 5, 10 and 15 wt% of TiO_2 weight in NiO-TiO_2 grains. The specimens were named as 2Ni-TiO_2, 5Ni-

TiO_2, 10Ni-TiO_2 and 15Ni-TiO_2 according to the Ni weight percent in the NiO-TiO_2 grains. Nomenclature for the sample name is adopted to emphasize on the variation of Ni weight percent in the composite grains.

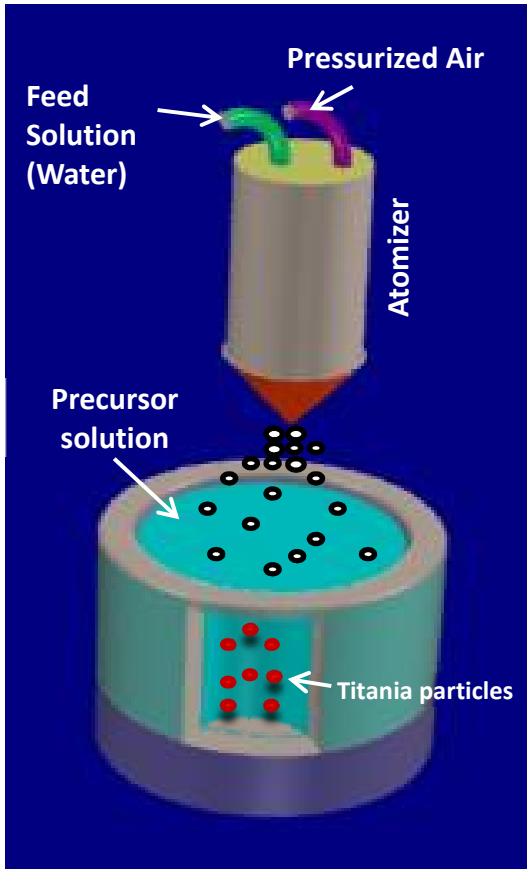

Fig. 1 *Schematic diagram of the spray hydrolysis method used for synthesizing TiO_2 submicrospheres.*

2.2. Fabrication of TiO_2/CNTs Composites

Catalytical chemical vapour deposition (CVD) method was used to synthesize the CNTs over the surface of the NiO-TiO_2 particles. NiO-TiO_2 microspheres, as prepared by spray hydrolysis, were reduced under hydrogen atmosphere at 600^{o}C for 30 min to get the Ni-TiO_2. One gram of different Ni-TiO_2 samples was taken in a ceramic boat and kept at the hot zone of the horizontal

quartz tube furnace. Initially, the furnace was flushed with argon gas (1 liter/min) to get the inert atmosphere inside the quartz tube, where the specimens were placed. When the desired temperature (850^{o}C) was obtained, the acetylene (C_2H_2) (100 sccm: where sccm stands for standard cubic centimeter per minute) gas along with Argon (500 sccm) and hydrogen gas (500 sccm) were allowed to pass through the sample containing boat for 30 min. After the deposition of CNT (in the form of black residue on the catalyst supported substrate) the furnace was cooled down and different CNT grown samples were collected. The collected samples were purified by using dilute solution of nitric acid. The purified samples were further analyzed.

2.3. Mesoscopic/Microscopic Characterization

Overall morphology of the grains has been investigated by scanning electron microscopy (SEM) with energy dispersive X-ray analysis using CAM Scan (UK) instrument. The microstructure of CNT-TiO_2 composite was analyzed by a transmission electron microscope (TEM, 2000FX JEOL).

In order to get insight into the internal morphology of the sub-microspheres, SAXS experiments have been performed on TiO_2 and the CNT composites using a laboratory based facility. It is important to mention here that SAXS technique is able to probe structures over a size range from approximately 1 nm to 100 nm [36]. Small-angle scattering experiment measures the scattered intensity versus the magnitude of scattering vector, q, which is defined as $q=4\pi\sin\theta/\lambda$, where 2θ is the scattering angle and λ is wavelength of the probing radiation. The sample to detector distance was kept 1.5 m and the available q-range was 0.1 to 2.2 nm^{-1}. Irreversible growth of nanoparticles (NPs) at higher temperature has also been monitored by SAXS experiments on the heat treated (600^{o}C for 4 hours) specimens. In order to probe the hierarchical structure of TiO_2 and CNT/TiO_2 grain, USANS experiments have been performed at S18 instrument [37] at

Institut Laue-Langevin, France using a Bonse-Hart camera by accessing smaller q. It is important to mention here that scattering data carry information in reciprocal space in contrast to microscopy which allows to access direct space. However, scattering experiments provides statistically averaged bulk sensitive information whereas electron microscopy is local probe of the matter and give only surface information. Thus, it is always advantageous to perform microscopy and scattering experiments simultaneously in order to obtain complementary information.

X-ray diffraction (XRD) experiments have been carried out to study the stability of Ni-TiO_2 composites at high temperatures. In-situ XRD experiments have been performed using a diffractometer (CuKα source) in θ-θ geometry with 2 deg/min scanning speed.

3. Results and Discussion

3.1. Electron Microscopy Results

Fig. 2 depicts SEM micrographs corresponding to TiO_2 grains doped at different NiO level. An agglomerated structure of fine grains is evident from micrographs. From image analysis of the micrographs, the typical size of the individual grains within the agglomerate is found to be 0.1 μm-1.0 μm. Fine grains tend to agglomerate due to attractive forces originating from van der Waal interaction. Similar morphology has also been observed for the virgin TiO_2 specimens synthesized under identical experimental condition [38]. The strength of Van der Waals force depends on the size of the aggregates. We believe that these aggregate may be destroyed if sufficient external energy is provided. The external energy could be in the form of mechanical forces such as ball milling etc. The un-agglomerated Ni-TiO_2 grains may be superior candidate for homogenous growth of CNT on the submicrosphere. Presence of NiO in the hydrolyzed TiO_2

grains is confirmed by energy dispersive x-ray (EDX) analysis of the specimens. The results of elemental analysis of the 10Ni-TiO_2 specimens are shown in Table-1.

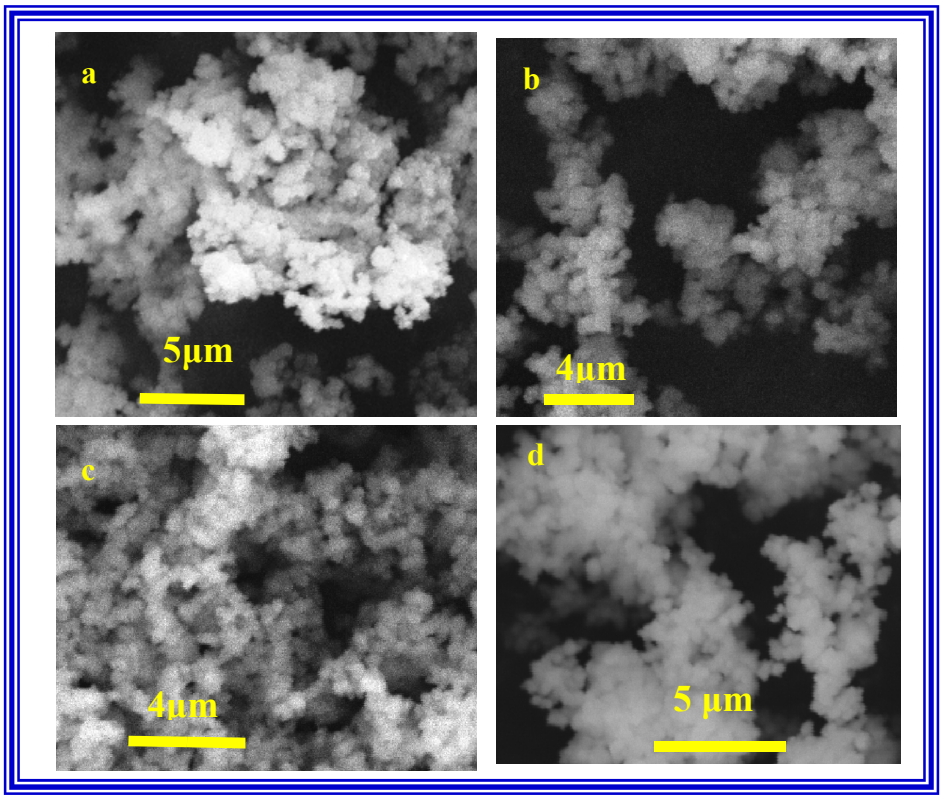

Fig.2 *SEM micrograph of (a) 2Ni-TiO_2 (b) 5Ni-TiO_2 (c) 10Ni-TiO_2 and (d) 15 Ni-TiO_2 specimens.*

Table- 1 *Elemental analysis from EDX of the 10Ni-TiO_2 grains is shown.*

Element	Weight percent	Atomic percent	Compd%	Formula
Ti K	53	31	88	TiO_2
Ni K	9	4	12	NiO
O	38	65		
Total	100	100	100	

In order to see detailed CNT microstructure, high resolution SEM and TEM experiments have been performed on TiO_2/CNT composites. High resolution SEM micrographs have been shown in Fig. 3. The presence of nanotubes is evident from the micrographs of the composite grains. It is evident from figure that 15CNT-Ni-TiO_2 shows homogeneous growth of CNT all over the Ni-TiO_2 substrate.

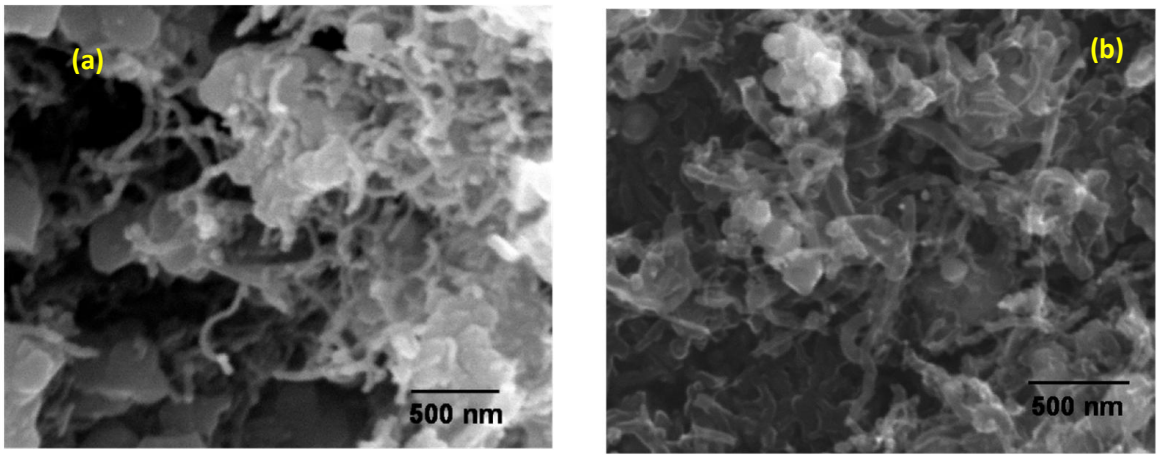

.

Fig. 3 *High resolution SEM micrographs of (a) 5Ni-TiO_2-CNT and (b) 15Ni-TiO_2-CNT composite grains are shown.*

The TEM micrographs for 5Ni-TiO_2-CNT and 15Ni-TiO_2-CNT are depicted in Fig. 4 and 5, respectively. It has been observed that CNT structure in 15Ni-TiO_2-CNT is more agglomerated as compared to nanotubes in 5Ni-TiO_2-CNT specimens. The TEM images clearly show that the nickel present on the surface acts the catalyst and surface of TiO_2 acts as the substrate from which the CNT grows. In case of 15Ni-TiO_2-CNT there were more sites present on the surface of TiO_2 leading to the agglomeration of CNTs. The TEM images shows that the diameter of CNT is around 40-60 nm.

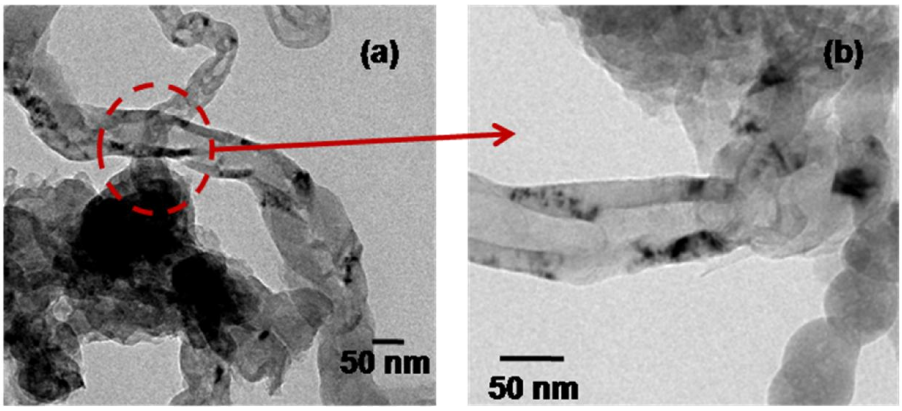

Fig. 4 *TEM micrographs of 5CNT-Ni-TiO_2 composite grains are shown. (a) Black spot shows the Ni-TiO_2 grains through which there was growth of CNT. (b) High resolution image shows the grown CNT from the agglomerate.*

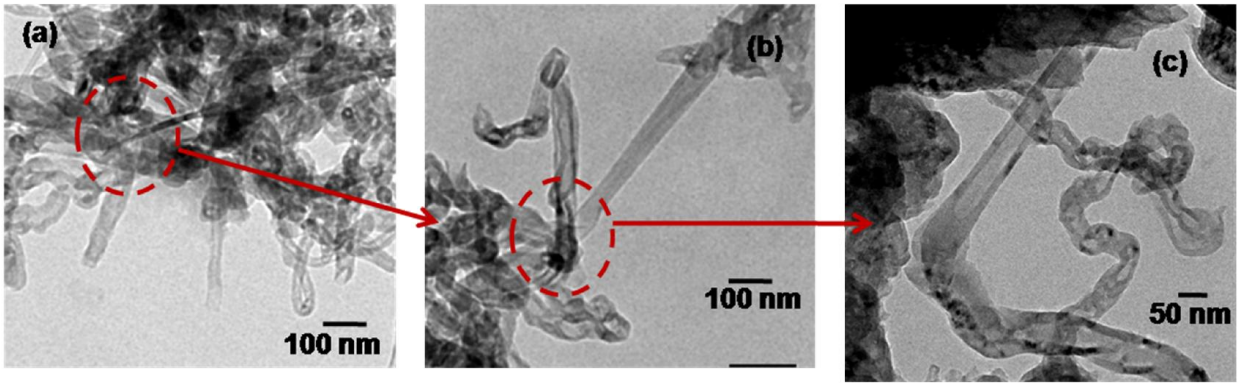

Fig. 5 *TEM micrographs (a) (b) & (c) of 15CNT-Ni-TiO_2 composite grains are depicted in different magnifications.*

3.2. SAXS Results

SAXS profiles, corresponding to the virgin and the heat treated NiO doped TiO_2 grains, are shown Fig. 6. Scattering profile for virgin TiO_2 grains is also depicted in Fig. 6 for comparison. The scattering profiles of heat treated specimens are quite different as compared to that of virgin

specimens. During heat treatment, growth of NPs occurs via atomistic diffusion that leads to a relatively sharp SAXS profiles for the heat treated specimens.

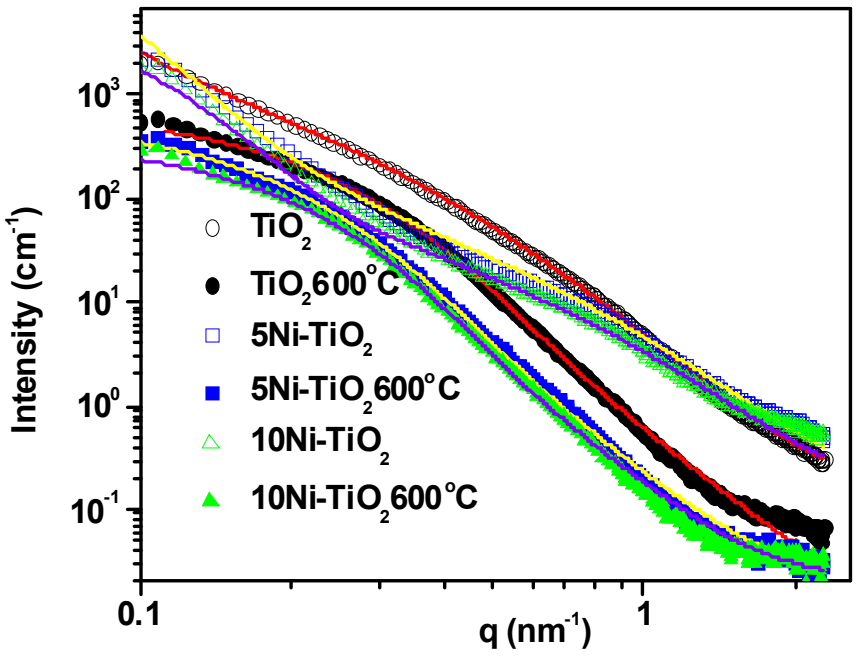

Fig. 6 *SAXS profiles of TiO_2, Ni doped TiO_2 and heat treated specimens. Solid lines are model fit to the data.*

The size of the TiO_2 NPs, resulting from hydrolysis process of the Ti-$(OR)_4$, depends on the medium of the hydrolysis. The size of the NPs may be controlled if the hydrolysis reaction is performed in acidic medium. This process is also some time referred as peptization process. More detail information about the peptization process can be found in the literature [39]. The addition of $Ni(NO_3)_2$ makes the hydrolysis medium acidic. This results into smaller size of the NPs as compared to the NPs formed without presence of $Ni(NO_3)_2$ as evident from the SAXS measurement.

The scattering intensity corresponding to an ensemble of polydisperse spheres can be expressed as [36]:

$$I(q) = n(\Delta\rho)^2 \int P(q,r)D(r)v_p{}^2 dr \qquad (1)$$

where, n is number density of the NPs, $(\Delta\rho)^2$ is the contrast factor and is defined as the electron density (scattering length density for neutrons) difference between NPs and matrix. Electron density of the matrix is assumed to be zero as experiments have been carried out in the powder form. Hence, $\Delta\rho$ in the present case is nothing but the electron density of doped TiO_2. P(q, r) is the spherical form factor and can be expressed [40] as below.

$$P(q,r) = 9\left[\frac{\sin(qr) - qR\cos(qr)}{(qr)^3}\right]^2 \qquad (2)$$

D(r) the size distribution of NPs. It is known that if several multiplicative factors are responsible for the growth of the NPs which is true for growth process in hydrolysis reaction, the size distribution should be of lognormal type. The expression for lognormal distribution may be written as below:

$$D(r) = \frac{1}{\sqrt{2\pi\sigma^2 r^2}}\exp\left[-\frac{\left(\ln(r/r_0)\right)^2}{2\sigma^2}\right] \qquad (3)$$

where r_0 is the median radius and σ is the polydispersity index of the size distribution. The average size can be expressed as $r_0\exp(\sigma^2/2)$.

It is observed that scattering profiles could not be fitted using mono-modal size distribution of NPs for virgin TiO_2 as well as doped TiO_2 grains. However, if bimodal distribution of NPs is

adopted, experimental profiles could be fitted satisfactorily. In such a situation, scattering intensity may be written as follows:

$$I(q) = C_1 \int P(q, r_1) \; V_P^{\,2} D_{larger}(r_1) dr_1 + C_2 \int P(q, r_2) \; V_P^{\,2} D_{smaller}(r_2) dr_2 \qquad (4)$$

where C_1 and C_2 are the q independent constants and are related to contrast factor and number density of NPs. The fitting of above model to the experimental data is quite good (Fig. 6). The estimated size distribution of NPs is shown in Fig. 7.

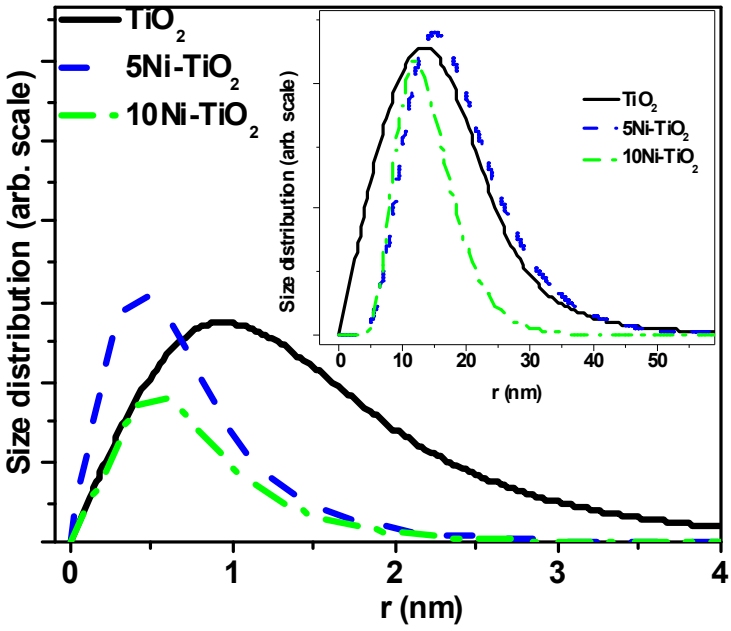

Fig. 7 *The primary TiO_2 NPs radius distribution, estimated by SAXS analysis. The inset shows the higher size contribution which may arise due to aggregation of primary NPs. r indicates the radius of the NPs.*

It is evident from Fig. 10 that TiO_2 NPs are polydisperse (~60%) in size. The average radius is ~1.5 nm. However, the average radius of the TiO_2 NPs for doped TiO_2 is less than 1 nm having

70% polydispersity in their size. The average radius of the aggregate of NPs is ~15 nm having ~50% polydispersity.

It is discernible that the scattering profiles of the heat treated specimens are somewhat sharper than that of the virgin one due to growth of NPs. The scattering profiles could be explained just by considering a mono-modal size distribution of NPs. The estimated size distribution is presented in Fig. 8. The size distributions of both virgin TiO_2 and Ni-TiO_2 NPs at high temperature are quite similar. It is evident from Fig. 8 that the radius of TiO_2 NPs increases to nearly 5 nm at 600^{o}C for all the specimens.

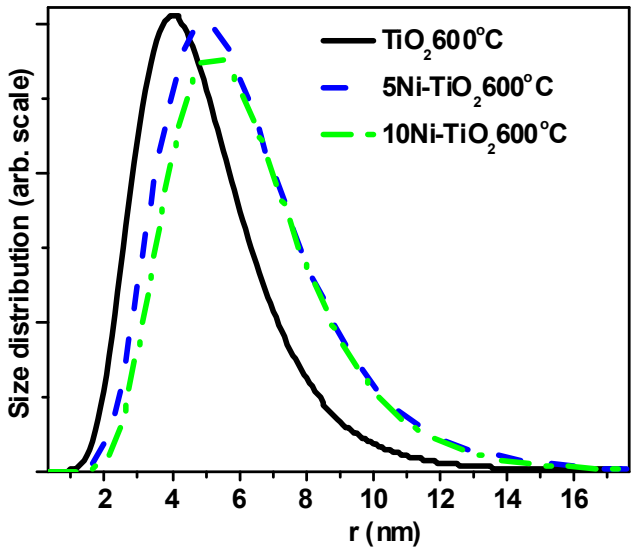

Fig. 8 *TiO_2 NPs size distribution for the specimens heated at 600^{o}C. ‘ r’ indicates the radius of the NPs.*

SAXS profiles of TiO_2/CNT composites are depicted in Fig. 9. It is discernible that the scattering profiles of the composite grains with respect to heat treated TiO_2 grains differ only at low q regime. It can be inferred from the above observation that SAXS profiles of the TiO_2/CNT

composites are mostly dominated by the scattering from TiO_2 NPs. It is worth mentioning here that during CNT fabrication, Ni-TiO_2 specimens underwent heat treatment at 800^oC.

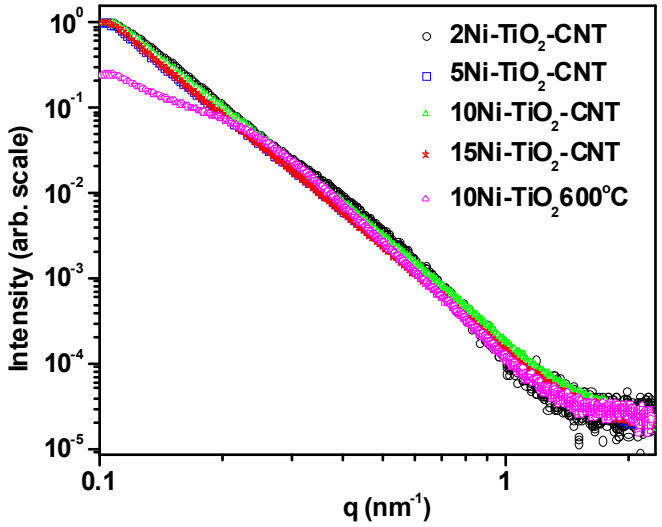

Fig. 9 *SAXS profiles of TiO_2/CNT composites in normalized scale at highest q.*

At this juncture, it is important to mention here that the small-angle scattering can provide the specific surface area information. Due to hierarchical nature of the composite grains, surface scattering contribution coming from each length scales. It is very difficult to differentiate the specific surface area at each length scale until the length scales are well separated. The specific surface area due to TiO_2 nanoparticles has been estimated for the Ni-TiO_2 grains from SAXS profiles. It is found that specific surface area varies from 100 m^2/gm to 60 m^2/gm for different specimens.

3.3. USANS Results

From Figs. 6 and 9, it has been observed that the scattering profiles for composite grains show an increasing trend even at the lowest accessible q. This indicates the existence of larger length scales, which is not accessible from SAXS experiment. Later on it will be shown that this is due to the presence of aggregated structure. In order to access higher length scales of composites grains, USANS experiments were performed. The experimental profiles are depicted in Fig. 10.

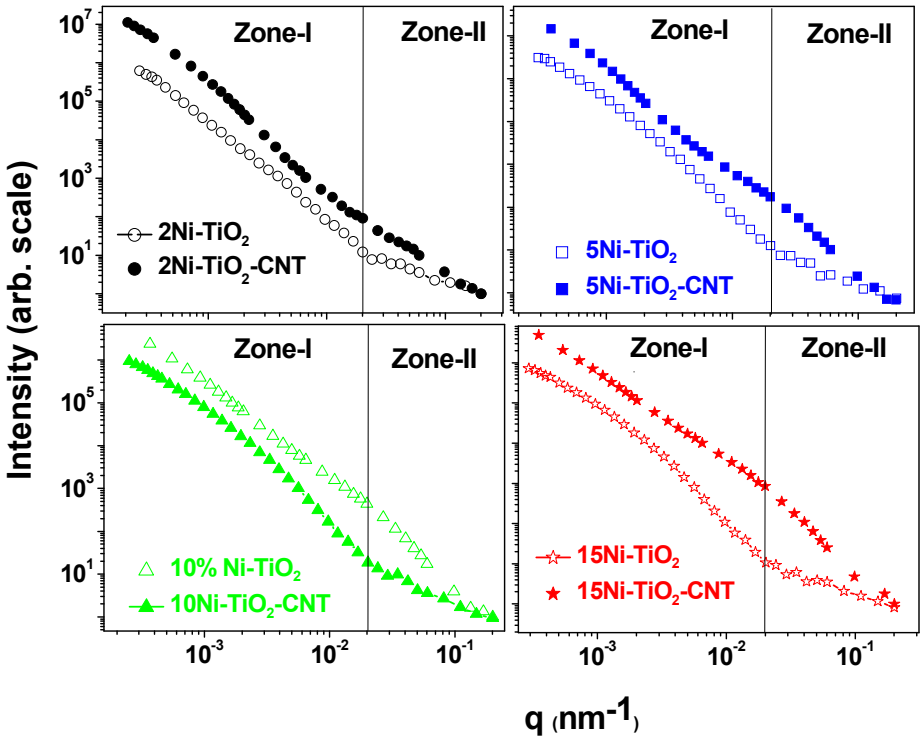

Fig. 10 *USANS profiles for the Ni-TiO_2 and TiO_2/CNT composites grains are depicted. The scattering profiles have been normalized at highest q of the data.*

It is evident from Fig.10 that scattering profile for TiO_2/CNT composite grains significantly differs as compared to that of only Ni-TiO_2 grains. The variation in the scattering profiles arises

due to growth of CNTs on Ni-TiO_2 grains. Doping of Ni in TiO_2 grains facilitates growth of CNTs during CVD. Hence, scattering contribution from CNTs increases with doping. Increase in yield of the CNTs with doping concentration is also confirmed by XRD measurements on composites and discussed in later section.

The USANS data for Ni-TiO_2 grains may be interpreted as follows. Zone-I of the scattering profile gives information about the individual grains and its correlation. It is assumed that the individual grains results from the hydrolysis of a single droplet. The Zone-II of the profiles contains the information about aggregates of NPs within the individual grains which is further supplemented and extended by SAXS experiments which is described in previous section. The scattering intensity from Zone-I has been modeled by accounting fractal correlation [41,42] between individual grains and may be approximated as

$$I(q) = C\left[\int D(r)V^2(r)P(q,r)dr\right]S(q, D_f, r_0, \xi) \quad (5)$$

where $S(q, D_f, r_0, \xi)$ is the structure factor corresponding to fractal like correlation between the individual grains. It can be expressed [41] as follows:

$$S(q, D_f, r_0, \xi) = 1 + \frac{1}{(qr_0)^{D_f}} \times \frac{D_f\Gamma(D_f - 1)}{\left[1 + \frac{1}{q^2\xi^2}\right]^{(D_f-1)/2}} \times \sin[(D_f - 1)\tan^{-1}(q\xi)] \quad (6)$$

where D_f is the mass fractal dimension, r_0 and ξ is the lower and upper cutoff lengths of fractal structure, respectively.

The size distributions of the individual grains, estimated from Zone-I, have been depicted in Fig. 11. Inset of Fig. 11 shows the model fit to the experimental data.

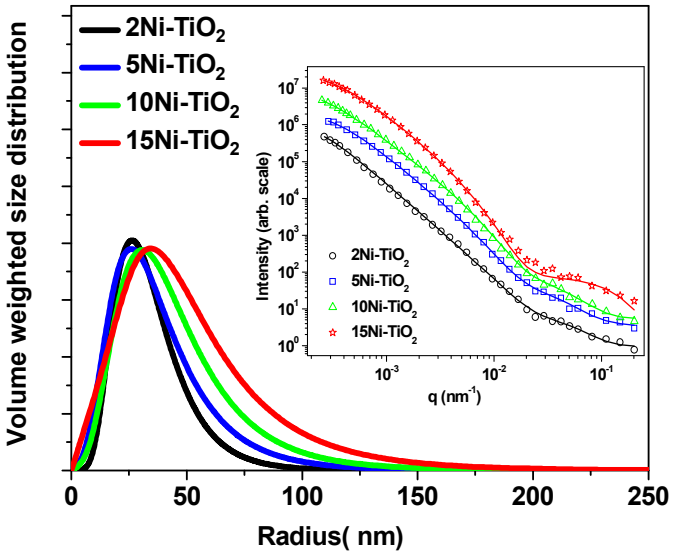

Fig. 11 *Size distribution of Ni doped TiO_2 grains as estimated from Zone-I of the USANS data. The inset shows the fitting of the USANS data using two level structure model. USANS profiles in the inset are shifted vertically for clarity.*

The average radius of the grains is found to be in the range of 35 nm to 52 nm for Ni-TiO_2 specimens, which corroborates with the TEM results. The radius of gyration [36], which is a measure of typical size of the agglomerate, is found to be 4-5 μm. By combing SAXS and USANS measurement, the hierarchical structure of the Ni-TiO_2 grains could be described in a quantitative fashion.

Zone-II of the scattering profiles has been modeled as an ensemble of polydisperse spheres (eq. 1). It is important to note that Zone-II of the USANS data overlaps with low- q SAXS data if proper scaling is carried out. Hence, the size distribution estimated from the Zone-II of USANS data and the size distributions of aggregate of NPs estimated from SAXS data (inset of Fig. 7)

are quite similar as expected. Few relevant parameters, obtained from USANS data analysis for Ni-TiO_2 grains, are tabulated in Table-2.

Table-2 *Parameter extracted from fitting USANS data of Ni-TiO_2 grains to the model*

	Contribution 1 (small aggregates of NPs)		**Contribution 2 NiO-TiO_2 submicrospheres**			
Doping concentration (wt %)	Average Radius (nm)	σ	Average Radius (nm)	σ	D_f	Radius of gyration R_g (μm)
2	16	0.39	35	0.44	2.4	4.9±0.3
5	14	0.51	40	0.55	2.3	3.8±0.3
10	15	0.50	45	0.54	2.2	4.6± 0.2
15	11	0.31	52	0.59	2.2	3.9±0.2

As discussed earlier that USANS data from CNT/TiO_2 grains are dominated by scattering from CNT structure except for 2Ni-TiO_2-CNT (where growth of CNTs is poor) specimen. The USANS data for the TiO_2/CNT composites have been explained as follows. The Zone-I of the data is dominated by scattering from aggregate of CNT nanostructures. Zone-II of the scattering data is prevailed by scattering from individual nanotubes. It is well known [43] that nanotubes dispersed or in powder form exhibit flexibility and often exist as agglomerated clusters even in well dispersed samples. Such aggregations may often be treated as a fractal in order to have a quantitative measure of the morphology of these aggregates. Small angle scattering is a convenient method to characterize such disordered aggregated or branched objects. CNTs in

composites grains have a cloud like fractal structure as is evident from the SEM micrograph. The USANS data of the CNT/TiO_2 composites have been modeled as an ensemble of cylinders having fractal correlation. The cross section radius of the cylinder has been assumed to be polydisperse in nature. The expression for the scattered intensity may be expressed by eq.5 where spherical form factor is substituted by cylindrical form factor Pc (q, r, L) with cross-section radius r and length L. The expression for the cylindrical form factor is [40],

$$P_c(q, r_0, L) = \int_0^{\frac{\pi}{2}} \left[\frac{2J_1(q\, r_0 \sin\alpha)}{q\, r_0 \sin\alpha} \frac{\sin((q\, L \cos\alpha)/2)}{(q\, L \cos\alpha)/2} \right]^2 \sin(\alpha) d\alpha \qquad (7)$$

where $J_1(x)$ is the first order Bessel function. The estimated radius distributions of the nanotubes are depicted in Fig. 12.

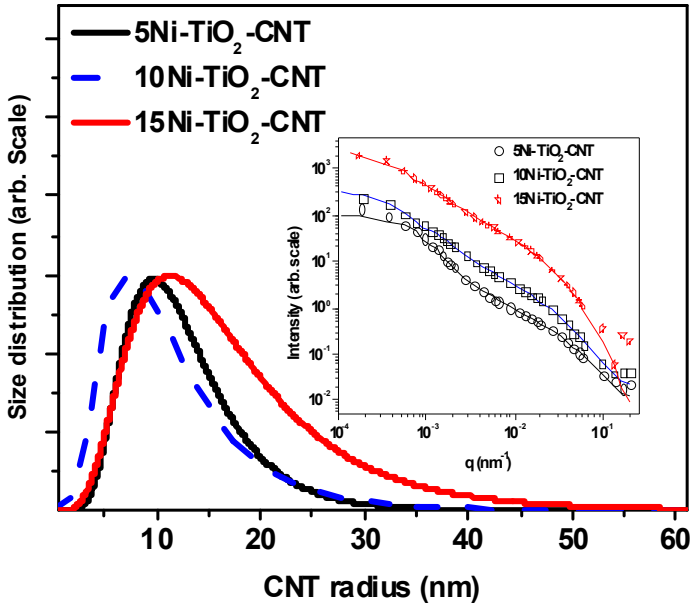

Fig. 12 *The estimated CNTs radius distribution form USANS data. The inset shows the USANS data with solid line as a fit.*

The inset of the figure shows the fitting of the model to the experimental data. The model agrees quite well with the experimental data. Few relevant fitting parameters, as obtained by USANS data analysis of the TiO_2/ CNT composite grains, have been tabulated in Table-3.

Table-3 *Important fitting parameter extracted from USANS data analysis of TiO_2/CNT grains*

Doping concentration (wt %)	CNT Structure		
	Average CNTs radius (nm)	σ	D_f
5	12	0.42	2.6
10	12	0.56	1.8
15	17	0.54	1.8

Radius of the CNTs for 5 wt% and 10 wt% is found to be approximately 10 nm. Average radius of CNTs increases with increasing doping. In addition to this, morphology of the nanotubes i.e. the correlation of the nanotubes gets modified at higher Ni concentration. The fractal dimension reduces significantly with increasing doping concentration indicating lesser compacted morphology of nanotubes at higher doping concentration.

3.4. X-ray Diffraction Results

XRD patterns at different temperatures for 5Ni-TiO_2 specimens are shown in Fig. 13.

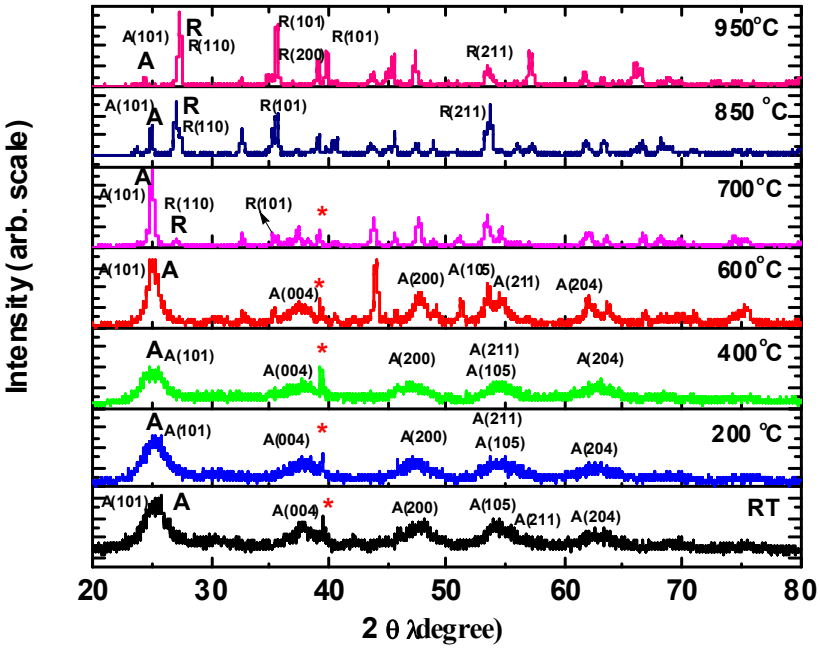

Fig. 13 *High temperature XRD patterns for the 5Ni-TiO_2 microspheres. A and R denotes the anatase and rutile phase, respectively.* marked peaks are due to the Pt sample holder. Anatase to rutile phase transition is observed beyond 600 ^oC.*

It is evident from the figure that TiO_2 is in anatase phase at lower temperature with substantial amorphous contribution. The observed diffraction profiles have been compared with the anatase and rutile phase of TiO_2 corresponding to JCPDS card nos. 21-1272 and JCPDS 21-1276, respectively. The indexing of the prominent peaks, corresponding to anatase and rutile phases, has been carried out. Some reflections at higher temperature could not be accounted by both anatase and rutile phases of titania. These peaks may correspond to some phase associated with compound of Ni. In present case, high temperature XRD experiments have been carried out in-situ which limits the collection of the XRD data for longer time. This results in to XRD patterns with lower resolution. Our interest in present work was to probe the stability of the composite

against anatase to rutile transformation. In future, we will try to understand the high temperature behavior of the materials and effect of the doping in detail way using high resolution XRD measurements.

The broadening of the peak is quite significant at lower temperatures. There is no clear phase transition of TiO_2 below 600oC. The weight fraction of anatase (W_A) and rutile (W_R) in both the specimens were calculated from the Spurr's equations [44]

$$W_A = \frac{1}{1+1.26\left(\frac{I_R}{I_A}\right)} \quad and \quad W_R = \frac{1}{1+0.8\left(\frac{I_A}{I_R}\right)} \tag{8}$$

where I_A and I_R are the intensities of peaks corresponding to (101) plane of anatase and (110) plane of rutile phase, respectively. The fractions of anatase and rutile phases, at different temperatures, have been tabulated in Table-4.

Table-4 *The parameters obtained from analysis of XRD patterns for 5Ni-TiO_2 specimen.*

Temperature (^{o}C)	**Weight percent**		**Average crystallite size of anatase phase (nm)**	**Average crystallite size of rutile phase (nm)**
	Anatase	**Rutile**		
27	100.0	-	4.1	-
200	100.0	-	3.8	-
400	100.0	-	3.8	-
600	100.0	-	7.2	-
700	93.3	6.7	19.3	14.6
850	35.5	64.3	30.1	19.2
950	8.9	91.1	34.5	30.4

Mean value of the crystallite size of anatase and rutile phases was calculated from the broadening of the X-ray reflections using the Scherer's formula [45]. The (101) crystallographic plane of anatase and (110) for rutile phase were considered for this purpose. It is evident from Table-4 that average anatase crystallite size of the virgin powder remains~ 4.1 nm and grows to ~7.2 nm at 600^{o}C. A rutile phase also appears at 700^{o} C with an average crystallite size of ~ 14.6 nm. The anatase crystallite size has been estimated to be 19.3 nm at 700^{o}C and it grows to 30 nm at 850^{o}C . The weight fraction of rutile phase increases with increasing temperature.

The TiO_2/CNT composites were also investigated by diffraction experiments. XRD patterns for the composite grains are shown in Fig. 14a.

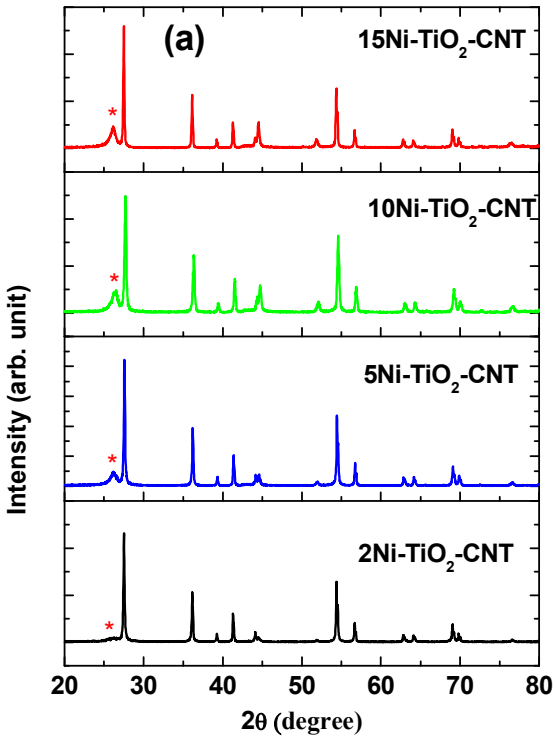

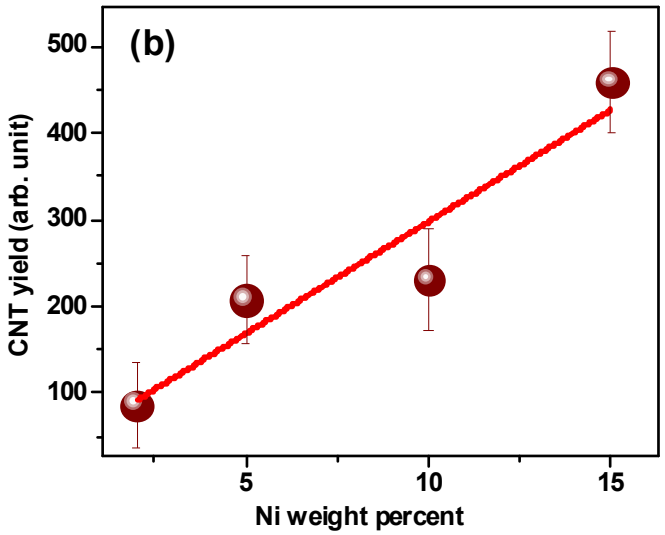

Fig. 14(*a)The XRD patterns of the CNTs grown on TiO_2 microspheres. The * marked peak corresponds to graphite peak of the CNT. (b) Yield of CNTs, as estimated from the peak intensity corresponding graphite peak, is shown with different Ni concentration.*

It is evident that TiO_2 in the composite grains exists in the rutile phase as Ni-TiO_2 grains were heat treated (~800^oC) during fabrication of CNTs. It is evident from figure that the intensity of the peak corresponding to graphite, increases with increasing Ni weight percent. Relative yields of CNTs have been estimated by XRD data by measuring peak position corresponding to the graphite and are presented in Fig. 14 b. It is evident from figure that the yield of CNTs increases with increasing Ni amount.

3.5. Formation of Submicrospheres

Let us understand the mechanism of formation of TiO_2submicrospheres:

The hydrolysis reaction for TTIP can be written as:

$Ti[OCH(CH_3)_2]_4 + 2\ H_2O \rightarrow TiO_2 + 4\ (CH_3)_2CHOH$

We consider a spherical water droplet surrounded by hexane phase containing TTIP (see Fig 15). Due to immiscibility between water and hexane, an interface is formed between water and hexane. TTIP comes into contact with water at interface only and hydrolysis reaction starts. Partially hydrolyzed TTIP, being hydrophilic, diffuses further into the water droplet. In the course of diffusion, partially hydrolyzed TTIP undergoes further hydrolysis reaction and condensation of resulting titanium hydroxide takes place resulting in the formation TiO_2 NPs. Diffusion of the hydrophilic hydroxide is limited to the droplet surface only if the concentration of TTIP is small leading to shell formation. In this case, hollow microsphere of TiO_2 is achieved [31]. For higher concentration of TTIP, partially hydrolyzed TTIP diffuses towards core of water droplet before condensation of titanium hydroxide takes place due to short supply of water molecule. Finally, localized condensation reactions take place inside water droplet not on the surface. Hence, shell formation and in turn formation of hollow sphere is most unlikely for this case. NPs forms in this process tend to aggregate due to its small size. Thus, individual grains resulting for the hydrolysis of single droplet consist of aggregated NPs. These grains get agglomerated further due to its submicron size. It is important to mention here that the aggregate of the NPs is quite stiff due to strong van der Waal attraction. However, the agglomerated structure of the grains is relatively soft due to weak van der Waal attraction. By combining results of microscopy (TEM and SEM) and scattering experiments, a simplistic mechanism for the formation of submicrospheres may be presented as shown in Fig. 15.

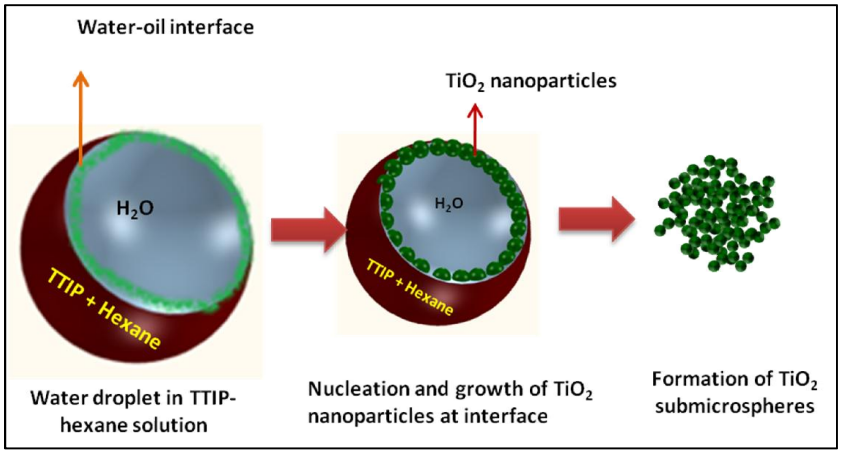

Fig. 15*The schematic representation of the mechanism for the formation TiO_2 submicrospheres during spray hydrolysis technique.*

4. Conclusions

Submicrospheres of NiO doped TiO_2 have been synthesized by spray hydrolysis technique. These hierarchical grains possess three level structures and have been investigated by scattering techniques. A plausible mechanism for the formation of submicrospheres from the droplet hydrolysis has been discussed. The diffraction experiment revels that initial phase of the TiO_2 NPs is anatase due its small size. Size of the NPs increases at higher temperature via atomistic diffusion and coalescence of NPs. Anatase to rutile phase transformation occurs for the TiO_2 NPs beyond 600^{o}C due to increase in size of NPs.

Synthesized Ni-TiO_2 grains have been utilized to prepare TiO_2/CNT composites using CVD route. The morphology of the nanotubes has been probed using microscopy as well as scattering techniques. It has been shown that the morphology of the nanotubes varies with Ni doping. The yield of CNTs also increases with increasing Ni content in the composite. We feel that Ni-TiO_2-CNTs composites may find applications in hydrogen generation via water splitting using photocatalytic property of the Ni-TiO_2. And subsequently, this composite may be used for

storage of hydrogen by utilizing high specific surface area of CNTs. The photocatalytic and hydrogen storage proper ties of the composites will be studied in near future.

References

1 A. Hagfeldt, M. Grätzel, *Chem. Rev.*, 1995, **95**, 49-68.

2 B. O'Regan, M. Grätzel, *Nature*, 1991, **353**, 737-740.

3 N. Sun Young, S. Ke, C. Chulmin, N. Mutong, Y. Muchuan, X. Ke, J. Sungho, W. Deli, *Nano Energy*, 2013, **2**, 351-360.

4 M. A. Fox, M. T. Dulay, *Chem. Rev.*, 1993, **93**, 341-357.

5 A. Fujishima, T. N. Rao, D. A. Tryk, *J. Photochem. Photobiol.C*, 2000, **1**, 1-21.

6 A. S. Gablenz, D. Voltzke, H. P. Abicht, J. N. Zdralek, *J. Mater. Sci. Lett.*, 1998, **17**, 537-539.

7 M. R. Hoffmann, S. T. Martin, W. Choi, D. W. Bahnemann, *Chem. Rev.*, 1995, **95**, 69-96.

8 A. Fujishima , K. Honda, *Nature*, 1972, **238**, 37-38.

9 A. L. Linsebigler, G. Lu, J. T. Yates, *Chem. Rev.*, 1995, **95**, 735-758.

10 K. Nagaveni, G. Sivalingam, M. S. Hegde, G. Madras, *Environ. Sci. Technol.*, 2004, **38**, 1600-1604.

11 J. C. Yu, J. G. Yu, W. K. Ho, Z. T. Jiang, L. Z. Zhang, *Chem. Mater.*, 2002, **14** , 3808-3816.

12 C. N. R. Rao, S. R. Yuganarasimhan, P. A. Faeth, *Trans. Faraday Soc.* 1961, **57**, 504-510.

13 J. Bahadur, D. Sen, S. Mazumder, P. U. Sastry, B. Paul, H. Bhatt, S. G. Singh, *Langmuir*, 2012, **28**, 11343-11353.

14 J. Bahadur, D. Sen, S. Mazumder, B. Paul, A. Khan, G. Ghosh, *J. Colloid Interface Sci.*, 2010, **351**, 357-364.

15 D. Eder, *Chem. Rev.*, 2010, **110**, 1348-1385.

16 I. Moriguchi, R. Hidaka, H. Yamada, T. Kudo, H. Murakami, N. Nakashima, *Adv. Mater.*, 2006, **18**, 69-73.

17 O. Frank, M. Kalbac, L. Kavan, M. Zukalova, J. Prochazka, M. Klementova, L. Dunsch, *Phys. Status Solidi b*, 2007, **244**, 4040-4045.

18 A. L. M. Reddy, S. Ramaprabhu, *J. Phys. Chem. C*, 2007, **111**, 7727-7734.

19 A. Kongkanand, R. Martinez Dominguez, P. V. Kamat, *Nano Lett.*, 2007, **7**, 676-680.

20 H. Song, X. Qiu, F. Li, *Electrochim. Acta*, 2008, **53**, 3708-3713.

21 H. Song, X. Qiu, F. Li, W. Zhu, L. Chen, *Electrochem. Commun*,. 2007, **9**, 1416-1421.

22 Y. Yao, G. Li, S. Ciston, R. M. Lueptow, K. A. Gray, *Environ. Sci. Technol.* , 2008, **42**, 4952-4957.

23 N. Bouazza, M. Ouzzine, M. A. Lillo-R´ odenas, D. Eder, A. Linares-Solano, *Appl. Catal. B*, 2009, **92**, 377-383.

24 Q. Shen, S.-K. You, S.-G. Park, H. Jiang, D. Guo, B. Chen, X. Wang, *Electroanalysis*, 2008, **20,** 2526-2530.

25 W. Karran, P. Georgios, S. Wolfgang, *Adv. Mater.*, 2009, **21**, 2233-2239.

26 J. Bahadur, D. Sen, S. Mazumder, J. Parkash, D. Sathiyamoorthy, R. Venugopalan, *J. Nanosci. Nanotechnol*,. 2010, **10**, 2963-2971.

27 A. Jitianu, T. Cacciaguerra, R. Benoit, S. Delpeux, F. Beguin, S. Bonnamy, *Carbon*, 2004, **42**, 1147.

28 C. S. Kuo, Y. H. Tseng, H. Y. Lin, C. H. Huang, C. Y. Shen, Y. Y. Li, S. I. Shah, C. P. Huang, *Nanotechnology*, 2007, **18**, 465607.

29 Q. Wang, D. Yang, D. M. Chen, Y. B. Wang, Z. Y. Jiang, *J. Nanoparticle Res*, 2007, **9**, 1087-1096.

30 W. D. Wang, P. Serp, P. Kalck, J. L. Faria, *Appl. Catal. B Environ.*, 2005, **56**, 305.

31 S. Nagamine, A. Sugioka, Y. Konishi, *Mater. Lett.*, 2007, **61**, 444-447.

32 H. Lakhotia, R. Singh, J. Bahadur, D. Sen, A. Das, S. Mazumder, B. Paul, P. Sastry, H. Lemmel, *J. Alloys Compd.*, 2014, **584**, 101-107.

33 S. Nagamine, S. Tohyama, M. Ohshima, H. Iwamoto, Y. Konishi, S. Tsukui, *J. Ceram. Soc. Jpn.*, 2009, **117**, 1158-1160.

34 B. Ahmmad, Y. Kusumoto, M. S. Islam, *Adv. Powder Technol.*, 2010, **21**, 292-297.

35 J. Bahadur, D. Sen, S. Mazumder, S. Bhattacharya, H. Frielinghaus, G. Goerigk, *Langmuir*, 2011, **27**, 8404-8414.

36 A. Guinier, G. Fournet, B. C. Walker, L. K. Yudowith, Small Angle Scattering of X-Rays, Wiley, New York, 1955.

37 M. Hainbuchner, M. Villa, G. Kroupa, G. Bruckner, M. Baron, H. Amenitsch, E. Seidl, H. Rauch, *J. Appl. Cryst.*, 2000, **33**, 851-854.

38 R. Singh, D. Sen, J. Bahadur, S. Mazumder, *AIP Conf. Proc.*, 2012, **1447**, 301-302.

39 Brian L. Bischoff, Marc A. Anderson, *Chem. Mater.*, 1995, **7**, 1772-1778.

40 J. S. Pedersen, *Adv. in Colloid and Interface Sci.*, 1997, **70**, 171-210.

41 J. Teixeira, *J. Appl. Cryst.*, 1988, **21**, 781-785.

42 H. D. Bale, P. W. Schmidt, *Phys. Rev. Lett.*, 1984, **53**, 596-599.

43 X. Zhao, Y. Ando, L.-C. Qin, H. Kataura, Y. Maniwa, R. Saito, *Appl. Phys. Lett.*, 2002, **81**, 2550-2553.

44 R. A. Spurr, H. Myers, *Anal. Chem.*, 1957, **29**, 760-762.

45 H. P. Klug, E. L. Alexander, X-ray diffraction procedures for polycrystalline and amorphous materials, J. Wiley and Sons, New York, 1974.